A novel antibacterial and biocompatible Ta-Ag coating fabricated by cold spray technology

Pengfei Yu, Shuo Yin, Rocco Lupoi
Department of Mechanical, Manufacturing and Biomedical Engineering, Trinity College Dublin, The University of Dublin, Parsons Building, Dublin 2, Ireland

Fergal J O'Brien, Katelyn J Genoud
Tissue Engineering Research Group, Royal College of Surgeons in Ireland, 123 St. Stephen's Green, Dublin 2, Ireland
Trinity Centre for Biomedical Engineering, Trinity College Dublin, Ireland
Advanced Materials and Biomedical Engineering Research (AMBER) Centre, Dublin, Ireland

Yingchun Xie
National Engineering Laboratory for Modern Materials Surface Engineering Technology; The Key Lab of Guangdong for Modern Surface Engineering Technology; Guangdong Institute of New Materials, Guangzhou 510651, China

Abstract

Infection caused by bacterial contamination is a critical problem challenging the successful use of medical implants in orthopaedic and dental applications. Consequently, medical implants with antibacterial abilities are in high demand. Tantalum and silver have been previously characterized to have excellent biocompatibility and antibacterial ability, but due to their significantly different properties, it is challenging to manufacture Ta-Ag components via thermal processing methods. Herein, by taking advantage of the unique characteristics of cold spray (CS) technology, an antibacterial Ta-Ag coating was successfully fabricated for the first time. In the CS process, blended Ta-Ag powders with different Ag concentrations were used to fabricate CS Ta-Ag coatings. Their antibacterial ability was preliminary tested and deposition behaviour was systematically investigated. The coating significantly reduced the metabolic activity of *S. aureus* bacteria, and a better deposition efficiency was obtained by blended Ta-Ag powder. It was found that soft Ag could aggregate in the coating and hard Ta particles were prone to rebound, which induced the peening effect for Ag and mass loss of Ta in the final coating Moreover, the clue of metallurgy bonding between Ta and Ag was detected in the region that experienced severe deformation despite their immiscibility.

Introduction

Cold spray (CS) is a solid-state deposition technology in which the deposition process can be achieved with a relatively low temperature in comparison to thermal spray(Ref 1,2). As schematically demonstrated in Fig.1, powder particles required for deposition are delivered into a high-pressure heated gas stream in the cold spray process. Then, the gas stream goes through a converging-diverging de-Laval nozzle and is accelerated to the supersonic velocity. At the same time, powder particles are also propelled to an ultra-high velocity. After that, powder particles will impact the substrate at a high speed. Depending on different gas parameters, the impact velocity usually ranges from 300 m/s to 1200m/s (Ref 3–5) For ductile particles, the high-velocity impact results in an extreme deformation on particles, which breaks the oxide layer on the surface of particles and creates a clear inter-particles or particle-substrate interface for metallurgical bonding. The ultra-high strain rate deformation that occurred in the region around the impact interface induces atomic diffusion and dynamic recrystallization, which causes metallurgy bonding. Whereas hard particles, like ceramic, will be directly embedded in the substrate, and deposition is achieved via mechanical bonding. Due to the special deposition mode of CS, high deposition efficiency can be easily achieved in CS.

In comparison to the thermal spray, there is no melting-solidification process in the CS deposition, which consequently minimizes the influence of high temperature on thermally sensitive materials, and the composition, phase, and properties of powder particles can be retained. Moreover, inert gas, like nitrogen and helium, is usually used as propellant gas, which simultaneously creates a protective atmosphere for powder particles and alleviates oxidation. Due to these features of CS, thermal and oxide-sensitive materials, have been appropriately deposited via CS(Ref 6–8) Furthermore, benefitting from diverse bonding mechanisms in CS, different composite deposits have also been successfully fabricated by CS (Ref 9,10). Even the composite deposits that consist of materials having extremely different properties, such as aluminium-alumina and aluminium-diamond, were produced by CS and presented excellent wear resistance and thermal conductivity (Ref 11–13) These successful applications of cold spray make it possible to design and fabricate some multi-functional composite coatings by using materials that have diverse properties.

It has been widely confirmed by vivo and in vitro testing that Ta has excellent biocompatibility and is also a bioactive metal. Orthopaedic implant devices made of Ta have been successfully applied in clinical practice (Ref 14,15). Moreover, Ag is an excellent inorganic antibacterial material and is less toxic for humans than other antibacterial metals like copper

(Ref 16). To minimize the risk of infection in orthopaedic implant surgery, great effort has been taken to fabricate Ag-containing composite coatings and alloys (Ref 17–19). However, using Ta as the matrix to fabricate Ag-containing coatings or components is still blank, which may be the consequence of great challenges induced by significantly different properties between Ta and Ag. Ta is a refractory metal having a melting point of 3290K which is higher than the boiling point of Ag, which means that it is impossible to fabricate Ta-Ag composites by using any approaches that have a melting process. Additionally, Ta is sensitive to oxide when the temperature is higher than 500℃ (Ref 20). Thus, a long period of vacuum or protective gas atmosphere is required for high-temperature processing methods. Although there is a significant difference in properties between Ta and Ag, both Ta and Ag have excellent ductility, which makes it possible to fabricate Ta-Ag composite deposits via cold spray. In this work, a Ta-Ag composite deposit having the function of biocompatibility and antibacterial ability was fabricated by the cold spray. Then, the antibacterial ability of coatings was tested and the deposition behaviour, as well as interparticle bonding mechanisms, were investigated.

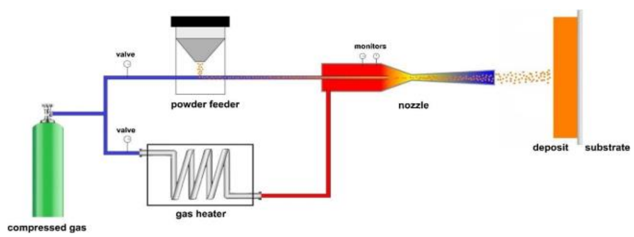

Fig.1 schematic of the cold spray process.

\

Materials and Method

In the cold spray process, gas atomized Ag powder (99% purity, Beijing Shouyi Metallic Material CO. Ltd.) and special grade pure Ta powder (99.9% purity H.C. Starck Inc, Germany) were used. Due to the significantly different densities between Ag and Ta, the impact velocity of Ta particles could be slower than that of Ag particles if a similar particle size were used, which may result in an inhomogeneous distribution of Ta and Ag in the deposit. To ensure Ag and Ta particles impact with similar velocity, a robust computational fluid dynamics (CFD) model was used to simulate the propelling process of Ag and Ta particles in the gas stream (Ref 21,22) Based on the CFD modelling results, the spherical Ag powder with the particle size ranging from 15μm to 50μm and angular Ta powder with particles size ranging from 10μm to 35μm were used in the cold spray. The CFD calculated velocity for the Ta powder was 395 m/s - 454 m/s and 454m/s-514m/s for the Ag powder. 2%, 5%, and 10% volume ratio of Ag powders were mechanically mixed with Ta powder, which is respectively named as Ta-2Ag, Ta-5Ag, and Ta-10Ag powder.

The cold spray process was conducted by using an in-house cold spray system available at Trinity College, Dublin. Nitrogen gas was used to propel powder particles. The inlet pressure of N_2 was 30 bar and the gas temperature was 600℃. Although higher gas temperature could lead to a better deposition of Ta, our previous attempts found that the nozzle could be severely clogged by Ag if the gas temperature was higher than 600℃. The de-Laval nozzle had a round cross-sectional shape with a divergent length of 180 mm. The throat and outlet diameters were 2 mm and 6 mm, respectively. A pure aluminium plate was used as the substrate. The stand-off distance was 40mm and the traverse speed was 800 mm/min. A 30×30mm deposition was fabricated by repeating each layer 6 times with an average feeding rate of 1.5g/s.

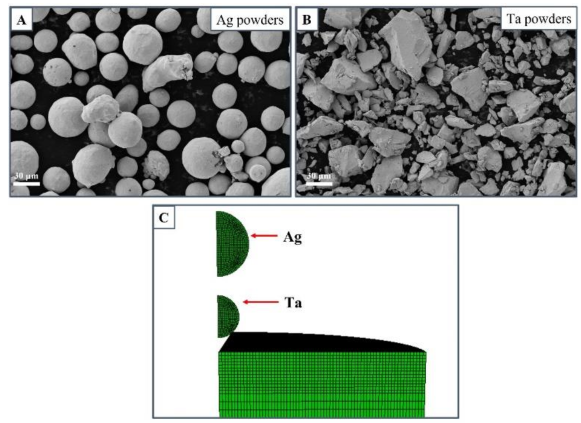

Fig.2 morphology of (A) Ag and (B) Ta powder particles, and the geometry model used in FEA modelling.

Ta-Ag deposits were cut by wire EDM to obtain their cross-section. Cut Ta-Ag deposits were ground and polished to obtain a mirror surface. Their cross-sections were observed with the Zeiss Ultra Scanning electron microscope (SEM) and the composition distribution was mapped by the Oxford Inca EDX detector. The hardness of Ta and Ag regions was also tested by using nanoindentation to find the changes in mechanical properties of Ta and Ag after the spraying. In the nanoindentation testing, the Berkowitz tip was used, and 20 indentation points were randomly selected both on Ta and Ag regions. Finally, Deposits were peeled off and fractured by bending. The fracture morphology was observed by SEM.

In addition to a series of testing, as shown in Fig.2C, a 3D multi-particle finite element analysis (FEA) model was built to simulate the high-velocity impact process in the cold spray, which can provide more information about the deformation process that cannot be obtained by experimental methods, In the FEA model, the starting velocity of the particle was 454 m/s for 30 μm Ag particle and 20 μm Ta particle. The initial temperature of the substrate was 293 K. The temperature of the Ag particle and Ta particle were 376K and 385K, respectively. The total modelling time was 100 μs. The plastic deformation behaviour of particles and substrate was described by Johnson-Cook constitutive relation, which is expressed as follows(Ref 23).

$$\sigma_y = (A + B\varepsilon_e^n)\left(1 + C\ln\frac{\dot{\varepsilon}}{\dot{\varepsilon}_0}\right)\left[1 - \left(\frac{T - T_0}{T_m - T_0}\right)^m\right] \quad (1)$$

ε_e is the equivalent plastic strain. T, T_0, and T_m are the reference and the melting temperature, respectively. Constants A, B, and C are material-related constants; n and m describe the strain-hardening and thermal-softening effects, respectively. The value of the parameters in Eq. (1) is given in the Table. 1

Table. 1 value of the Johnson-Cook model for Ta and Ag (Ref 24).

Material	A (MPa)	B (MPa)	C	n	m	$\dot{\varepsilon}_0$ (s^{-1})	T_0 (K)
Ta	684	205	0.043	0.78	0.34	1	300
Ag	60	168	0.03	0.325	1.28	1	298

Table. 2 physical, thermal, and mechanical parameters of Ta and Ag used in the FEA simulation.

Parameter	Ta	Ag
Density (kg/m^3)	16690	10490
Young's Modulus (GPa)	186	83
Poisson Ratio	0.34	0.37
Thermal Conductivity (W/m/K)	57.5	406
Specific Heat (J/kg/K)	140	234
Melting Temperature (K)	1235	3290

To validate FEA modelling results and have a deeper investigation of the deposition behaviour, a single-splat experiment was also conducted. To make sure both the deposition of Ag and Ta particles be observed, 50% Ag volume Ta-Ag powder was used in a single-splat experiment. The powder was separately deposited on Ag and Ta substrate with a rapid traverse velocity. Then, features of a single splat and deposition of single particles were observed via SEM. With the assistance of FEA modelling, the deposition process in CS can be rebuilt.

Being different to the plate-count method, in this work, a more accurate metabolic evaluation was taken to evaluate antibacterial ability. The culturing 5×10^5 CFU/mL *S. aureus* Newman (CFU = colony forming units- a common measurement to express the number of bacteria) on the samples for 24 hours at 37°C. After which the samples were rinsed 3 times with phosphate buffered saline (PBS) and then incubated in a 10% alamar blue solution in the culture broth (Brain Heart Infusion (BHI) broth) for 1 hour at 37°C protected from light. Finally, 100 µl (microliters) of each sample in triplicate were plated in a black 96 well plate and absorbance was measured at 570nm and 590nm as per manufacturer's instructions.

Results and discussion

Features of Ta-Ag deposits

Fig.3 shows the EDS mapping of the Ta-Ag deposit cross-section and Fig.4 is the deposition efficiency in the cold spray of different Ag volume ratio Ta-Ag powder. It can be seen in Fig.3 that the distribution and morphology of Ag in the CSed Ta-Ag deposit changed with Ag volume in powder. In Fig.3A and B, when the Ag volume was 2% and 5%, Ag was separately dispersed in the Ta matrix and some Ag segments were highly deformed into the plate shape. Although the Ag volume in the powder increased from 2% to 5%, the volume of Ag in the Ta-2Ag and Ta-5Ag deposits did not increase obviously. On the contrary, when Ag volume increased to 10%, as presented in Fig3C, large Ag agglomerates were formed in the Ta matrix and some small Ta segments were randomly dispersed in large Ag agglomerates like islands.

The variation deposition efficiency demonstrates interesting results. The deposition efficiency of pure Ta is 30%, and it started to decrease with adding more Ag from 2% to 5%. However, when the volume of Ag increased to 10%, the deposition efficiency rapidly raised to 40%. This variation tendency is usual. Because it has been widely reported that in the cold spray process, the addition of soft particles in the hard particles powder the deposition efficiency can be improved and increase with the volume of soft particles. In addition to deposition efficiency, the reduction of Ta volume in final Ta-Ag deposits was found. Fig.4A shows the Ag volume in starting powders and final CSed Ta-Ag deposits. It is seen that the Ag volume in the deposit made of Ta-2Ag and Ta-10Ag powder were 3.23±0.67% and 21.27±0.53% respectively, which were both higher than that in the starting powder. However, the Ag volume in the deposit made of Ta-5Ag powder was 4.18±0.92%, which was almost equal to the Ag volume in the starting powder.

Fig.5 shows the hardness of Ta and Ag region in the composite Ta-Ag deposit with different Ag volumes. It can be seen that the hardness of Ta regions in the composite deposit has no significant change in comparison to the pure Ta deposit. However, the Ag region in the Ta-Ag deposit gained higher hardness after cold spray than pure Ag. It should be noted that both Ta and Ag in Ta-5Ag demonstrate the highest hardness in the final deposit, which indicates the more significant strain hardening induced by the peening effect on Ta-5Ag.

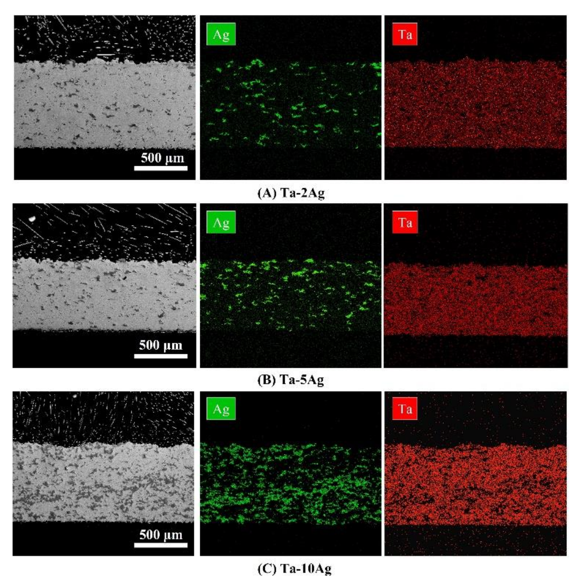

Fig.3 SEM and EDS mapping images of the cross-section of Ta-Ag deposits fabricated with different Ag volume powders. (A) 2% Ag, (B) 5% Ag, (C) 10% Ag.

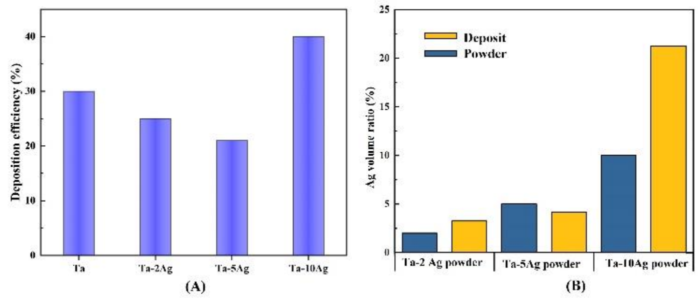

Fig.4 (A) deposition efficiency and (B) Ag volume ratio in the powder and final deposit.

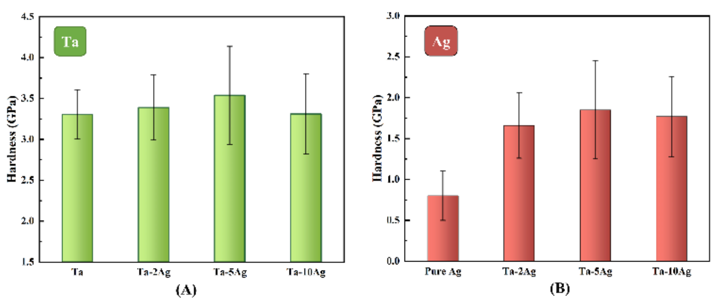

Fig.5 average hardness of Ta and Ag region in the final deposits.

Antibacterial ability

Fig.6 presents the metabolic activity of *S. aureus*. The addition of Ag can reduce the metabolic activity of *S. aureus*. But the antibacterial ability was not monotonically enhanced with the Ag volume increasing. On the contrary, the medium Ag volume deposit, Ta-5Ag, shows the largest metabolic activity reduction but not Ta-10Ag.

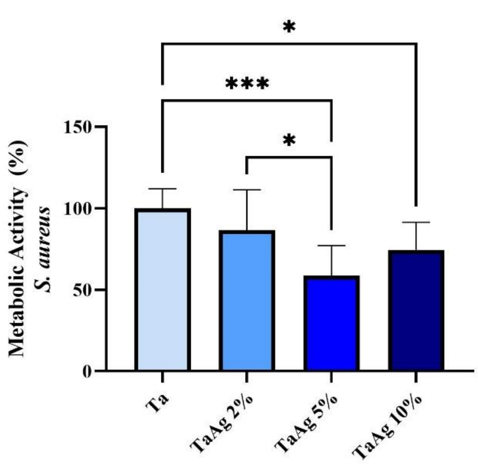

Fig 6 changes of metabolic activity of S. aureus in different Ag volume surface.

Deposition behaviour for mixed Ta-Ag powder in CS

The CSed Ta-Ag deposit presents some abnormal results both in the deposit itself and its antibacterial ability, which may be related to the deposition behaviour of mixed Ta-Ag powder in the cold spray process.

The extreme processing condition in the CS results in a great challenge to obtain real-time information about particle deformation. Thus, the FEA modelling was applied. Based on the volume of Ag in the mixed powder, in the FEA modelling the deposition situation can be simplified into two modes, which are Ta onto Ag particles then onto Ta substrate and Ta onto Ag then onto Ag substructure, which respectively corresponds to low Ag volume and high Ag volume. In the following text, two conditions were all named as Ta-Ag-Ta(sub) and Ta-Ag-Ag(sub)

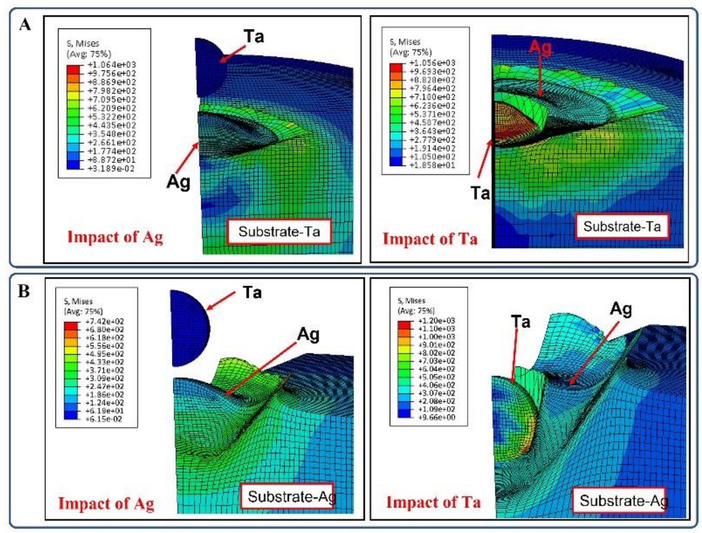

Fig.7 FEA model of different deformation in the cold spray. (A)Ta-Ag-Ta(sub) and (B) Ta-Ag-Ag(sub).

Fig 7 shows the 3D modelling result. As shown in Fig.7A, in the Ta-Ag-Ta (Sub) condition, when Ag impact on the Ta substrate severe deformation occurred on the Ag particle and jetting dramatically formed on the periphery. But on the Ta substrate side, less deformation happened. When the Ta particle sequentially impacted on Ag segment, Ta particles embedded in the Ag particles and Ag experienced more deformation. However, due to the small volume of Ag particles, the Ta particle cannot embed deeper and be trapped by Ag. At the same time, Ag absorbs the majority kinetic energy of Ta, like a sponge. No deformation occurred on the Ta particle. Moreover, the impact of Ta particles induces extra kinetic energy for Ag, and Ag segments were knocked out by the Ta particles.

The modelling result was further proved by the single splat experiment. As shown in Fig.8A, angular Ta particles successfully deposit on the Ta substrate because of appropriate deformation on both sides of the Ta particle and substrate. In Fig.8B, it can be seen that the Ag particle was severely deformed into the shape of a plate, but less deformation happened on the Ta. On the contrary, many round craters were formed on the Ta, which indicates the rebound of Ag particles.

As for the multi-particle impact condition, in Fig.8D, craters can be seen on a large Ag particle. According to the size and the angular shape of the crater, they were formed by the rebound of Ta particles, which matches well with the modelling results shown in Fig.7A.

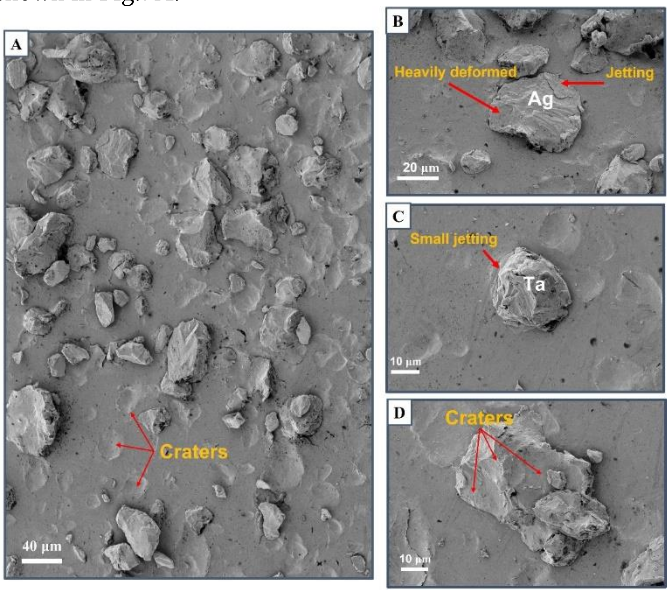

Fig.8 single splat experiment of Ta-Ag-Ta(sub) condition.

On the contrary to low Ag volume powder, if the Ag volume is enough high to generate large Ag agglomeration, the deformation condition changes into Ta-Ag-Ag(Sub) and the deposition behaviour also varied. As shown in Fig.7B, when an Ag particle impacts the Ag substrate, the jetting structure formed on both sides of the Ag particle and substrate, which indicates that Ag is easy to achieve metallurgy bond in CS. That is the reason why large Ag agglomerations are highly formed in Ta-10Ag. Being different from Ag particles, when Ta particles sequentially impact on the Ag, due to the higher hardness of Ta, they are deeply embedded into the Ag. But less deformation occurred on the Ta particle. This deformation condition further affects deposition the process in CS. Fig.9 shows the deposition process of Ta-Ag-Ag(sub) mode in a single splat. Being the same with FEA modelling, Jetting occurred on both sides of the Ag particle and previously deposited Ag, and excellent bonding was achieved. In contrast, some Ta particles were deeply embedded in the Ag and got trapped. However, not all the particles got trapped after embedding into Ag. Some of Ta particles rebound from the Ag surface and left angular craters, which lead to the reduction of Ta in the final deposits.

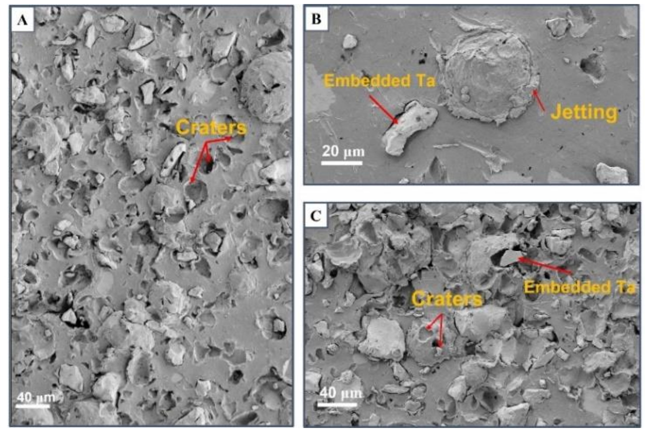

Fig.9 single splat experiment of Ta-Ag-Ta(sub) condition.

Based on the finding above, the deposition behaviour in Ta-Ag cold spraying process is schematically demonstrated in Fig.10.

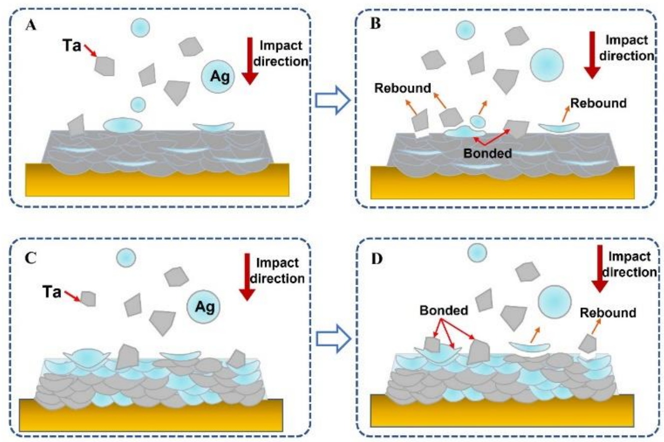

Fig.10 schemes of depositions process with different volumes of Ag in powder. (A) and (B) for Ta-2Ag and Ta-5Ag, (C) and (D) for Ta-10Ag.

When the Ag volume was 2%, due to the large amount of Ta, its deposition mode was similar to pure Ta powder. Metallurgical bonding occurred between the Ta particles, but due to the imperfect CS parameter, the deposition efficiency was low. For Ag particles, owing to the less deformation on the Ta side and immiscibility between Ta and Ag, Ag particles were easy to rebound. However, a large amount of Ta particles induced a hammering effect on Ag particles, and severer deformation occurs on both sides of Ag and Ta, which let some Ag particles bond with Ta and led to the formation of lamellar Ag in the final Ta-Ag deposit.

When the Ag volume increased to 5%, although Ag got more chance to deposit on the previous layer, 5% of Ag was not enough to form a large Ag agglomerate. On the contrary, the formation of a small Ag agglomerate deteriorated the deposition. Firstly, in the deposition, because of insufficient bonding strength between Ag and Ta, smaller Ag agglomerates were easy to be knocked out in the impact of the following particles. Secondly, small Ag agglomerates cannot trap Ta particles well. However, they absorbed the kinetic energy of Ta particles and let Ta particles experience less deformation, which further makes metallurgy bonding between Ta and Ag, especially considering the immiscibility between Ta and Ag. Consequently, Ta particles are easy to rebound. Finally, the bonding between Ta particles also was still limited by the unsatisfied CS parameter. In general, these factors worked together and resulted in a worse deposition for 5% Ag powder.

If the Ag volume increased to 10%, Ag particles got more chance to deposit, and large Ag agglomerates formed in the Ta-Ag deposit. The formation of Ag agglomerates not only promoted the deposition of Ag via metallurgy bonding but also offered suitable mechanical bonding conditions for Ta particles. In general, a higher Ag volume in powder could significantly improve the deposition efficiency of Ta-Ag powder. However, because the bonding strength resulting from mechanical bonding is weaker than metallurgical bonding, some Ta particles rebound. Because of it, the volume of Ag in the Ta-10Ag deposit was higher than Ta.

Influence of deposition behaviour on antibacterial ability

Although there are still some arguments on the antibacterial mechanism of Ag, it is no doubt that silver ion release from materials is crucial for antibacterial ability. The release of ions from metal or ceramic is related to crystal defects including dislocation and grain boundary (Ref 25,26). It is found that a high dislocation density or small grain size (large volume of grain boundary) can promote the release of ions in the materials. (Ref 25–28)

In the cold spray process, severe deformation induced by the high-speed impact can significantly increase dislocation density and refine the grain size to the nanoscale. On the macro level, the increase of crystal defects results in higher hardness for materials. It is interesting to find that the hardness of Ta and Ag are both improved after the cold spray and the improvement is most obvious for Ta-5Ag. As discussed above, the deposition efficiency of Ta-5Ag powder is the lowest and the Ag in Ta-5Ag experienced a more severe peening effect than Ta-10Ag. Additionally, Ta-5Ag has higher Ag volume that Ta-2Ag.

Generally, the peening effect induced more crystal defects for Ta-5Ag than Ta-10Ag and a higher volume of Ag than Ta-2Ag, which may result in the best silver release ability for the Ta-5Ag deposit. However, based on the present result the conclusion above is doubtful, more detailed testing and characterization will conduct in future work.

Bonding mechanisms for Ta-Ag deposits

The deposition behaviour of powders usually depends on the bonding mechanism among the powder. In the practice, due to the continuous impact of particle bonding mechanisms including mechanical and metallurgy will occur with the input of deformation. Ta and Ag are a unique combination due to their immiscibility and significant difference in mechanical properties. The bonding mechanism in the cold spray of Ta-Ag mixed powder is investigated and discussed in this section.

Fig.11 is the SEM images and corresponding EDS results of the cross-section of Ta-10Ag deposits. It can be seen that a large Ag region embedded in the Ta matrix, and in the boundary between Ta and Ag vortex structure formed. the vortex structure is the consequence of severe deformation induced by the continuous impact of sequentially impact particles on ductile Ag. The vortex plays a crucial role in the bonding between the immiscible Ta and Ag system Because the vortex structure could offer robust mechanical bonding between Ag and Ta. Furthermore, the EDS mapping and point analysis on point I, shown in Fig 11C and D, prove that Ag and Ta could diffuse into each other in the arm of vortex structures, which indicates that metallurgy bonding may occur between Ag and Ta despite the immiscibility between them.

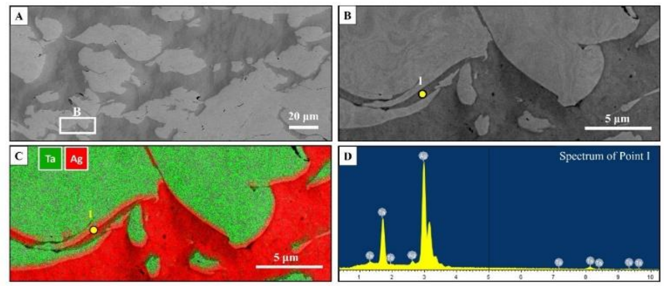

Fig.11 SEM images and EDS of the cross-section

To further investigate the bonding mechanism, the fracture surface of the Ta-Ag deposit obtained by bending was observed via SEM and presented in Fig.12. In Fig.12A, clear dimple structures can be found in the region circled by orange square, which is further proved as Ag in EDS testing. In addition to the dimples, a sharp blade structure also formed on Ag after the fracture, which was formed by the necking of the vortex structure when the Ag vortex was subjected to tensile strength. The dimples and blade structure on Ag indicate that ductile fracture is the predominant fracture mode for Ag, which also proves that Ag particles are bonded via metallurgy bonding. In comparison to Ag, the fracture surface of Ta is smooth, and cleavage can be found, which suggests the brittle fracture mode among Ta particles.

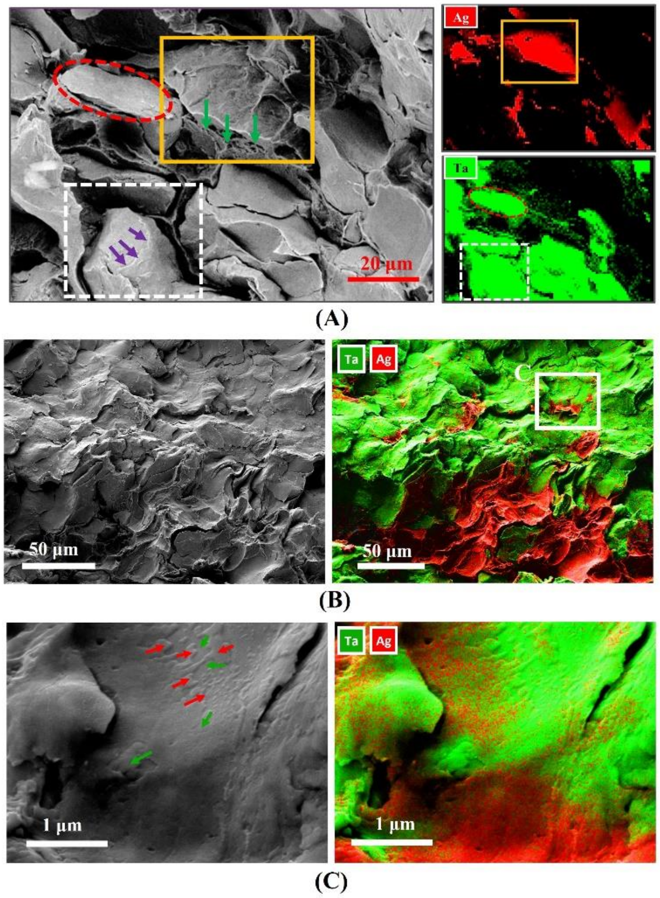

Fig.12 SEM images and EDS mapping of fracture morphology of Ta-Ag deposits.

As shown in Fig.12B, there are some Ag agglomerates dispersing on the Ta. A more detailed observation was conducted on the region circled by white squares and respectively presents in Fig.12C. In Fig.12C, it is interesting to find some flakes marked by red arrows attaching to a smooth surface. The EDS mapping indicated that flake structures are some Ag peeled off from Ag and attached to the Ta surface. In general, based on the SEM and EDS analysis, in addition to mechanical interlocking, metallurgy bonding occurred in the Ag vortex structure but not in the smooth Ta-Ag interface. The possible reason for the occurrence of metallurgy bonding between Ta and Ag is given as follows.

Ta-Ag system has a positive enthalpy of solution and consequently be recognized as an immiscible alloy system(Ref 24). However, if there is enough energy input into the system, the energy barrier can be overcome, and then Ag and Ta can diffuse into each other. Herein, the particle impacted with an ultra-high kinetic energy that was then transferred into thermal and strain energy. But the kinetic energy of a single particle cannot induce enough energy to overcome the energy barrier and trigger the diffusion process. Thus, there was no metallurgy bonding detected in the smooth Ta-Ag interface. However, in the vortex structure, due to the continuous impact of particles, Ta, and Ag, both went through a severer deformation. With the impact process going on, the deformation energy gradually exceeds the energy barrier. With the assistance of raised temperature, the Ta and Ag atoms were further thermally activated and diffused into each other. Finally, immiscible Ta and Ag particles were bonded via metallurgy bonding.

Conclusion

In this work, Ta-Ag composite deposits were successfully fabricated by cold spray technology. The fabricated Ta-Ag composite deposit has higher hardness and good antibacterial ability. Moreover, the deposition behaviour and bonding mechanism are investigated and obtained following conclusion. Firstly, it is found that when the volume of soft particles is small, more soft particles do not always result in better deposition efficiency for hard-soft mixed powder in cold spray. Herein When the volume of soft Ag particles is lower than 10%, the deposition efficiency did not increase with Ag volume. 5% volume of Ag resulted in the worst deposition due to the rebound of Ta and a smaller volume of Ag agglomeration.

Secondly, the predominant bonding mechanism in Ta-Ag cold spray is mechanical interlocking. Additionally, despite the immiscibility between Ta and Ag, the formation of the vortex structure not only can induce better mechanical bonding but also can lead to metallurgy bonding due to higher deformation energy input during the formation of the vortex structure.

The higher crystal defects induced by the higher peening effect on Ta-5Ag powders could result in higher Ag ion release, which further improves antibacterial ability. However, at present, it is still challenging to explain the usual excellent antibacterial ability of Ta-5Ag deposit. it may relate to the deformation condition and substructure distribution, for example, dislocation and voids, in Ag, which needed further investigation.

Acknowledgements

The authors are grateful for the financial support from the China Scholarship Council (No.202006220041) and from Science Foundation Ireland (grant 12/RC/2278).

References

1. H. Assadi, F. Gärtner, T. Stoltenhoff, and H. Kreye, Bonding Mechanism in Cold Gas Spraying, *Acta Mater.*, 2003, **51**(15), p 4379–4394.
2. H. Assadi, H. Kreye, F. Gärtner, and T. Klassen, Cold Spraying–A Materials Perspective, *Acta Mater.*, Elsevier, 2016, **116**, p 382–407.
3. T. Schmidt, F. Gärtner, H. Assadi, and H. Kreye, Development of a Generalized Parameter Window for Cold Spray Deposition, *Acta Mater.*, 2006, **54**(3), p 729–742.
4. A.A. Tiamiyu, Y. Sun, K.A. Nelson, and C.A. Schuh, Site-Specific Study of Jetting, Bonding, and Local Deformation during High-Velocity Metallic Microparticle Impact, *Acta Mater.*, Pergamon, 2021, **202**, p 159–169.
5. W.-Y. Li, H. Liao, C.-J. Li, G. Li, C. Coddet, and X. Wang, On High Velocity Impact of Micro-Sized Metallic Particles in Cold Spraying, *Appl. Surf. Sci.*, 2006, **253**(5), p 2852–2862.
6. T. Liu, M.D. Vaudin, J.R. Bunn, T. Ungár, and L.N. Brewer, Quantifying Dislocation Density in Al-Cu Coatings Produced by Cold Spray Deposition, *Acta Mater.*, 2020.
7. M.R. Rokni, C.A. Widener, A.T. Nardi, and V.K. Champagne, Nano Crystalline High Energy Milled 5083 Al Powder Deposited Using Cold Spray, *Appl. Surf. Sci.*, 2014, **305**, p 797–804.
8. P.C. King, C. Busch, T. Kittel-Sherri, M. Jahedi, and S. Gulizia, Interface Melding in Cold Spray Titanium Particle Impact, *Surf. Coatings Technol.*, 2014, **239**, p 191–199.
9. A.W.-Y. Tan, J.Y. Lek, W. Sun, A. Bhowmik, I. Marinescu, P.J. Buenconsejo, Z. Dong, and E. Liu, Microstructure, Mechanical and Tribological Properties of Cold Sprayed Ti6Al4V–CoCr Composite Coatings, *Compos. Part B Eng.*, 2020, **202**, p 108280.
10. X. Chu, H. Che, C. Teng, P. Vo, and S. Yue, A Multiple Particle Arrangement Model to Understand Cold Spray Characteristics of Bimodal Size 316L/Fe Powder Mixtures, *Surf. Coatings Technol.*, Elsevier, 2020, **381**, p 125-137.
11. R. Fernandez and B. Jodoin, Cold Spray Aluminum–Alumina Cermet Coatings: Effect of Alumina Morphology, *J. Therm. Spray Technol.*, 2019, **28**(4), p 737–755.
12. B. Aldwell, S. Yin, K.A. McDonnell, D. Trimble, T. Hussain, and R. Lupoi, A Novel Method for Metal–Diamond Composite Coating Deposition with Cold Spray and Formation Mechanism, *Scr. Mater.*, 2016, **115**, p 10–13.
13. R. Nikbakht, H. Assadi, K. Jahani, M. Saadati, and B. Jodoin, Cold Spray Deformation and Deposition of Blended Feedstock Powders Not Necessarily Obey the Rule of Mixture, *Surf. Coatings Technol.*, Elsevier, 2021, **424**, p 127644.
14. J.M. Schierholz, L.J. Lucas, A. Rump, and G. Pulverer, Efficacy of Silver-Coated Medical Devices, *J. Hosp. Infect.*, Elsevier, 1998, **40**(4), p 257–262.
15. H. Matsuno, A. Yokoyama, F. Watari, M. Uo, and T. Kawasaki, Biocompatibility and Osteogenesis of Refractory Metal Implants, Titanium, Hafnium, Niobium, Tantalum and Rhenium, *Biomaterials*, Elsevier, 2001, **22**(11), p 1253–1262.
16. B.R. Levine, S. Sporer, R.A. Poggie, C.J. Della Valle, and J.J. Jacobs, Experimental and Clinical Performance of Porous Tantalum in Orthopedic Surgery, *Biomaterials*, Elsevier, 2006, **27**(27), p 4671–4681.
17. M. Kikuchi, M. Takahashi, T. Okabe, and O. Okuno, Grindability of Dental Cast Ti-Ag and Ti-Cu Alloys, *Dent. Mater. J.*, The Japanese Society for Dental Materials and Devices, 2003, **22**(2), p 191–205.
18. K.-H. Liao, K.-L. Ou, H.-C. Cheng, C.-T. Lin, and P.-W. Peng, Effect of Silver on Antibacterial Properties of Stainless Steel, *Appl. Surf. Sci.*, Elsevier, 2010, **256**(11), p 3642–3646.
19. M. Chen, E. Zhang, and L. Zhang, Microstructure, Mechanical Properties, Bio-Corrosion Properties and Antibacterial Properties of Ti–Ag Sintered Alloys, *Mater. Sci. Eng. C*, 2016, **62**, p 350–360,
20. T. Van Steenkiste and D.W. Gorkiewicz, Analysis of Tantalum Coatings Produced by the Kinetic Spray Process, *J. Therm. Spray Technol.*, Springer, 2004, **13**(2), p 265–273.
21. M. Meyer and R. Lupoi, An Analysis of the Particulate Flow in Cold Spray Nozzles, *Mech. Sci.*, Copernicus GmbH, 2015, **6**(2), p 127–136.
22. M.C. Meyer, S. Yin, K.A. McDonnell, O. Stier, and R. Lupoi, Feed Rate Effect on Particulate Acceleration in Cold Spray under Low Stagnation Pressure Conditions, *Surf. Coatings Technol.*, 2016, **304**, p 237–245.
23. G.R. Johnson, A Constitutive Model and Data for Materials Subjected to Large Strains, High Strain Rates, and High Temperatures, *Proc. 7th Inf. Sympo. Ballist.*, 1983, p 541–547.
24. J. Kim, G. Bae, and C. Lee, Characteristics of Kinetic Sprayed Ta in Terms of the Deposition Behavior, Microstructural Evolution and Mechanical Properties: Effect of Strain-Rate-Dependent Response of Ta at High Temperature, *Mater. Charact.*, 2018, **141**, p 49–58.
25. T. Hanawa, Metal Ion Release from Metal Implants, *Mater. Sci. Eng. C*, 2004, **24**(6), p 745–752.
26. S. Dittrick, V.K. Balla, N.M. Davies, S. Bose, and A. Bandyopadhyay, In Vitro Wear Rate and Co Ion Release of Compositionally and Structurally Graded CoCrMo-Ti6Al4V Structures, *Mater. Sci. Eng. C*, 2011, **31**(4), p 809–814.
27. R. Kumar and H. Münstedt, Silver Ion Release from Antimicrobial Polyamide/Silver Composites, *Biomaterials*, 2005, **26**(14), p 2081–2088.
28. R. Hamai, S. Sakai, Y. Shiwaku, T. Anada, K. Tsuchiya, T. Ishimoto, T. Nakano, and O. Suzuki, Octacalcium Phosphate Crystals Including a Higher Density Dislocation Improve Its Materials

Osteogenecity, *Appl. Mater. Today*, 2022, **26**, p
101279.